RESEARCH ARTICLE | JANUARY 13 2026

The weakly bound CO molecule adsorbed on the low-index CeO_2 surfaces: A case for a CCSD(T) benchmark study using an embedded-cluster model

Juana Vázquez Quesada

J. Chem. Phys. 164, 024706 (2026)
https://doi.org/10.1063/5.0292423

The Journal of Chemical Physics ARTICLE pubs.aip.org/aip/jcp

The weakly bound CO molecule adsorbed on the low-index CeO_2 surfaces: A case for a CCSD(T) benchmark study using an embedded-cluster model

Cite as: J. Chem. Phys. 164, 024706 (2026); doi: 10.1063/5.0292423
Submitted: 22 July 2025 • Accepted: 8 November 2025 •
Published Online: 13 January 2026

Juana Vázquez Quesada[a)]

AFFILIATIONS

Institut für Nanotechnologie, Karlsruher Institut für Technologie (KIT), Kaiserstraße 12, 76131 Karlsruhe, Germany

[a)]Author to whom correspondence should be addressed: juana.quesada@kit.edu

ABSTRACT

The binding energy and the vibrational stretching frequency of the probe molecule CO adsorbed on the low-index CeO_2 surfaces [(100), (110), and (111)] were benchmarked using the coupled-cluster singles, doubles, perturbative triples [CCSD(T)] method, employing an embedded cluster approach. Using the same methodology as for the top configuration of CO on the (111) surface [J. Vázquez Quesada *et al.*, J. Chem. Phys. **161**, 224707 (2024)], the best theoretical estimate for the CO frequency on the CeO_2(100) surface (CO bridge configuration) obtained at the CCSD(T)/def2-TZ/QZVPP level of theory and under low-coverage conditions (2193 cm^{-1}) is 17 cm^{-1} larger than the experimental value (1 ML coverage saturation), which is in agreement with previous estimates for the CO adsorption on the CeO_2(111) surface (12 cm^{-1}). For the (110) surface, theoretical and experimental data compare differently. The CCSD(T)/def2-TZ/QZVPP values are −7 cm^{-1} (top configuration) and −21 cm^{-1} (tilt-*x* configuration) lower than the two experimental features measured at 2170 cm^{-1} (negative feature) and 2160 cm^{-1} (positive feature). MP2 predictions suggest the existence of a case of multiple-configuration dynamics with various almost isoenergetic configurations in a low-coverage situation. The CO harmonic vibrational frequencies were not semi-empirically scaled but explicitly corrected for anharmonic effects, which amount to 25–26 cm^{-1} with all tested methods. CO adsorption energies of −0.40 ± 0.07 eV, −0.17 ± 0.07 eV, and −0.20 ± 0.07 eV for the (100), (110) (top), and (110) (tilt-*x*) adsorption sites, respectively, are obtained at the CCSD(T)/def2-TZ/QZVPP level of theory. These results agree well with those proposed for the (111) surface (−0.22 ± 0.07 eV) [J. Vázquez Quesada *et al.*, J. Chem. Phys. **161**, 224707 (2024)] and confirm the physisorption character of the adsorption of CO on the three low-index surfaces of CeO_2.

I. INTRODUCTION

Any attempt to contribute to the establishment of reference data for the characterization of vibrational features of molecules adsorbed on metal and metal oxides requires two main contributions: first, experimental techniques to provide a precise settlement of these spectroscopic features for various adsorbates; and second, a theoretical methodology to interpret, support, and clarify at the molecular level the adsorbate–surface interaction.

In the experimental area, infrared reflection absorption spectroscopy (IRRAS) has been very successful in investigating the vibrational features of different molecules on metal and metal oxide surfaces, despite the challenges related to reflection and refraction that arise when working with dielectric surfaces.[1–4] It has been essential, however, to conduct measurements on true macroscopic single crystals, or mono-crystals, to provide consistent and more accurate information about surface dynamics.[5] This raises the need for monitoring characteristic shifts of vibrational bands of probe molecules for establishing "highly" accurate reference data. In this regard, carbon monoxide (CO) possibly represents one of the most prominent examples. A reliable assignment of CO vibrational frequency, or rather the shift with

respect to the gas phase frequency, has become a standard to be tested.[6,7]

Regarding the theoretical methodologies, there exist models based on the Born–von–Kármán periodic boundary condition (PBC),[8–10] which capture the properties of bulk, surfaces, and chains by repeating a single (primitive) unit cell in three, two, and one dimensions, respectively. In surface studies, a slab periodic model is constructed, allowing the treatment of surface relaxation for a given electronic structure method, usually density functional theory (DFT), and making possible a careful examination of high surface concentration of adsorbed molecules—the so-called high coverage.[9,10] For low coverage molecular adsorption, however, a large super-cell is required to minimize the interactions of the adsorbate units on the surface, causing the periodic models to become computationally expensive, especially if hybrid functionals or wavefunction-based correlation methods are employed.

Even though the application of methods such as coupled-cluster singles and doubles with perturbational treatment of triple excitations [CCSD(T)] to materials by imposing periodic boundary conditions has been pursued during the last years (see Refs. 11–14 and references therein), the high computational demand has made its routine application difficult. The latter has made necessary the development of different reduced-scaling techniques—for example, the local natural orbital (LNO) coupled-cluster (CC) method (LNO-CC) (see Refs. 15 and 16 and references therein). Alternatively, there exists the finite cluster model approach, which selects a part of the extended system, the so-called quantum-mechanical (QM) cluster, and where medium- and long-range interactions between the QM cluster and the rest of the extended system are simulated by means of one or another embedding scheme.[14,17–22] This quantum-mechanical (QM) cluster model enables the use of many of the currently available advanced wavefunction-based quantum-chemical methods for molecules, being a very valid approach when the molecule-surface phenomena is well localized.

Once experimental techniques and theoretical approaches are available, a substrate on which a large number of molecules can be adsorbed is necessary. This is the case for some metal and rare earth oxides[23–25] and undoubtedly for cerium dioxide (CeO_2, ceria).[26–31] The latter plays a significant role in fields such as film formation, solid oxide fuel cells,[32] biology,[33] components of emission control systems,[34,35] and heterogeneous catalysis. In this latter area, its importance is clearly distinct by its redox properties in reactions[2,27,34,36,37] and its dual use as a catalyst and as a support.[34] The investigation of molecules adsorbed on CeO_2 surfaces has gained relevance as a means to study electron transfer processes, surface reactions, and the presence of vacancies and dopants.[38,39]

Focusing on the three low-index CeO_2 surfaces—that is, (111), (110), and (100)—and taking CO as a probe molecule, for which there exists a sound set of experimental data,[5,7,40–42] the spectral range between 2140 and 2180 cm^{-1} still stays, even after years of work, under discussion. The stretching CO vibrational frequency is identified with CO bound perpendicular or tilted to the surface, with CO adsorbed on a more or less reduced surface (Ce^{4+} vs Ce^{3+}), and with CO adsorbed more or less close to surface oxygen vacancies.[43–45] To shed light on the wide range of possibilities, different theoretical studies using periodic DFT have been carried out during the last decades, trying to explain and confirm the experimental evidence. On this matter, the most comprehensive investigations have been carried out by Ganduglia-Pirovano *et al.* (see Refs. 46–53 and references therein), concluding both experiment and theory in a blueshift of the vibrational frequency of CO adsorbed on the three oxidized and reduced low-index surfaces of ceria.[49,51]

At this point, it is worth mentioning that CO is weakly bound to the CeO_2 surfaces,[54] i.e., often called "physisorbed." Thus, the prediction of vibrational frequencies and binding energies, significantly smaller than those of chemisorption cases, with a particular degree of accuracy, represents a significant challenge. Physisorption is distinguished by two types of interaction, viz., dispersion and classical electrostatics. In other words, electron correlation plays a central role, and a consistent treatment requires the use of wavefunction-based post-Hartree–Fock methods such as those based on Møller–Plesset perturbation (MP) or Coupled-Cluster (CC) theory.

For ionic systems—as in the case of CeO_2—the embedded cluster approach can be an alternative where the QM cluster is embedded in a grid of point charges (PCs) playing the role of the remaining part of the crystal. The boundary region between these PCs and the QM cluster is represented by pseudo-potentials (effective core potentials, ECPs), which occupy the position of the positive point charges. These ECPs avoid over-polarization of the cluster or charge transfer to the point charge field. This electrostatic embedding model has been applied to investigate oxygen vacancies in metal-oxides,[55,56] as well as adsorption energies of H_2O, NH_3, CH_4, CH_3OH, and CO_2 on different surfaces.[57,58] In the case of ceria, electrostatic embedding models have also been applied to CeO_2 bulk[17,59] as well as the (111)[17,60–62] and (110)[63–67] surfaces, including the computation of the CO binding energy on the (110)[63,65–67] and (111)[60–62] surfaces and of the CO vibrational frequency in the case of its adsorption on the CeO_2(110) surface.[63,65]

In relation to the use of post-Hartree–Fock methods, only early studies that applied the method of increments[68–70] to estimate the CO@CeO_2(111) and CO@CeO_2(110) binding energies calculated from partial energy contributions computed at the MP2 and CCSD(T) level of theory have been reported.[60,67] In addition to this, our group has recently published a benchmark study on the adsorption of CO on CeO_2(111), including correlated methods such as MP2 and canonical CCSD(T) in conjunction with the periodic electrostatic embedded-cluster model (PEECM)[17,71,72] to predict the CO binding energy and vibrational frequency. Furthermore, in the latter study, an explicit correction for anharmonic contributions to the CO stretching frequency was included.[62] In the present work, this benchmark model is extended to the adsorption of CO on the other two low-index surfaces of CeO_2, i.e., (110) and (100).

This article is organized as follows: Sec. II covers the methodology and technical details applied in this work. Results are presented in Sec. III. Section III A analyzes the influence of the size and shape of the clusters used in the embedding model when predicting the CO harmonic vibrational frequency. Computed harmonic CO stretching frequencies as well as anharmonic effects are further elaborated in Sec. III B. The CO binding energies are discussed in Sec. III C. Finally, Sec. IV summarizes the present work.

II. QUANTUM-CHEMICAL METHODS

As in our recent study on CO adsorption on $CeO_2(111)$,[62] optimized bare surfaces for $CeO_2(110)$ and $CeO_2(100)$ were taken from the literature (Ref. 51). In Ref. 51, the slab layer model in conjunction with the super cell approach[73] and using the PBE[74] functional, within the generalized gradient approximation (GGA), along with a Hubbard U-like term[75] (U = 4.5 eV for the 4f states of Ce), as well as the HSE06 functional,[76–79] was employed. For the (100) polar surface, the *checkerboard* (100)-O termination (4O–4Ce–8O···4Ce–4O) was considered.[51] Setting up the point charge field directly from the above-mentioned structure for the (100) surface led to a dipole moment perpendicular to the surface. This issue was solved by including additional charges at some distance from the adsorption site and according to the PEECM scheme.[17] The tested surfaces have cell sizes of (1 × 1) and (2 × 2) with calculated lattice constants of 5.485 Å (PBE+U)[51] and 5.398 Å (HSE06)[51] for the bulk ceria (Fm3m space group). All embedded calculations in the present work were carried out employing the Turbomole program package.[80] In particular, the second-order Møller–Plesset perturbation theory (MP2)[81] as well as the coupled-cluster singles and doubles with perturbational treatment of triple excitations [CCSD(T)][82] methods in conjunction with the Karlsruhe def2-SVP, def2-TZVPP, and def2-QZVPP basis sets[83,84] were utilized in this work. Basis sets with the inclusion of diffuse basis functions, i.e., def2-SVPD, def2-TZVPPD, and def2-QZVPPD,[85,86] were also used with the MP2 method. In all post-Hartree–Fock methods, the resolution-of-the-identity approximation (also called density fitting) was applied. While optimized auxiliary basis sets presented in Refs. 85 and 87–89 were used in most cases , for the D-basis sets of cerium, the auxiliary basis sets were constructed based on the procedure described in Ref. 90. A scalar-relativistic effective small core potential (ECP) of the Wood–Boring (WB) type covering the inner 28 electrons[91] was included in all calculations with "def2" basis sets for cerium. For energies and Cartesian gradients, convergence thresholds of $10^{-10}E_h$ and $10^{-10}E_h/a_0$, respectively, were used. To guarantee a numerical accuracy better than 1 cm^{-1} for the vibrational frequencies computed from numerical first and/or second derivatives of the potential energy, the convergence criterion of the energy with respect to the previous iteration and the Euclidean norm of the residual for the iterative solution of the coupled-cluster equations were set to 10^{-10}. Although for most of the post-HF methods the core electrons were not correlated (fc), core–valence electron correlation effects were investigated at the MP2 level correlating all electrons (ae) and using the correlation consistent polarized *weighted* core–valence basis sets (cc-pwCVnZ, n = D,T)[92] for carbon (C) and oxygen (O), as well as the cc-pwCVDZ-X2C and cc-pwCVTZ-X2C basis sets[93] for cerium (Ce). For consistency, the "def2" ECP for cerium and the corresponding optimized auxiliary basis sets[90,94] were also employed in building those for cerium according to the procedure presented in Ref. 90. For all the embedded-model computations, the automated periodic electrostatic embedding method (PEECM)[17] as implemented in the Turbomole program package[80] was employed. In this approach, the embedding is created by adding terms to the Fock or Kohn–Sham matrix using and distinguishing two parts within the interactions between the QM cluster and the point charge field, that is, the near-field (NF) interaction terms, which are computed by direct integration, and the far-field (FF) interaction terms evaluated by employing the multipole expansion of the Coulomb interactions[95–97] and by means of the fast multipole method.[98–100] In order to prevent polarization effects in the area between the QM cluster and the point charges, a boundary region was created at points where the Ce^{4+} ions closer to the QM cluster are located. This region was built with the electrostatic core potential (ECP) ecp-18-mhf[101] for Ti^{4+}, ions given that its ionic radius is similar to that of Ce^{4+}. In addition, the rest of the point charge field was represented by charges of +4 for Ce and −2 for O. The periodic electrostatic embedding cluster model (PEECM)[17] also includes additional charges to achieve a rapid and correct convergence.[61,71,72,102,103] The harmonic stretching frequency of the CO molecule adsorbed on all the embedded clusters studied in this work was numerically computed from analytic gradients when applying the MP2 method. For the CCSD(T) computations, this frequency was evaluated from an HF-Hessian obtained from analytical gradients with correlation contributions estimated by means of double numerical differentiation of energy points using central differences of gradients obtained by central differences, which results in $(6N)^2$ energy points (with N being the number of atoms). Displacements of 0.002 a_0 were applied. The accuracy of the numerical procedure was verified with the analytical procedure at the MP2 level, obtaining an agreement better than 1 cm^{-1}. Using a one-dimensional representation of the anharmonic potential along the CO vibrational normal coordinate, the anharmonic contribution to the potential energy was evaluated by numerical integration employing a Gauss–Hermite quadrature and reaching convergence with 13 grid points.[104]

III. RESULTS AND DISCUSSION

It has been well established in the literature that the low-index ceria surfaces follow the stability sequence (111) > (110) > (100).[105] The nonpolar (111) surface is characterized by an open structure with oxygen in the first layer, followed by a cerium layer and a building O–Ce–O sequence in the *z* direction. This surface exhibits only one type of Ce^{4+} ions with a sevenfold coordination, i.e., Ce is bound to seven oxygen atoms [Fig. 1(a)].[106] The CO molecule adsorbed on $CeO_2(111)$ shows an experimental stretching vibrational frequency at 2154 cm^{-1}.[107] Our most recent benchmark study,[62] as well as multiple other investigations[42,49,51,53,107,108] have confirmed that in this case, CO is adsorbed on top of the Ce^{4+} ion and almost perpendicular to the surface.

The nonpolar (110) surface is characterized by having both Ce and O atoms in the top layer; it is marked by three rows (O–Ce–O) at the first layer with the Ce^{4+} cations coordinated to two O^{2-} ions in the first layer and to four in the second [see Fig. 1(b)]. The IRRAS-SLIR experiments of CO adsorbed on the oxidized (110) surface show two peaks blueshifted with respect to the CO frequency in the gas phase.[109] In particular, a strong negative band at 2170 cm^{-1} (+27 cm^{-1} shift) and a positive, less intense feature at 2160 cm^{-1} (+7 cm^{-1} shift) are observed.[108] This surface has been the most controversial regarding the possible CO adsorption sites. Already, the first theoretical studies[63,64] using an embedding model and the DFT functional B3LYP explored five adsorption sites, of which two resulted in being distinctly more stable. In one, CO was located above a Ce^{4+} ion in the first layer in a position slightly tilted to the surface, resulting in a CO harmonic frequency blueshifted with respect to that of CO in the gas phase. In the other, CO was

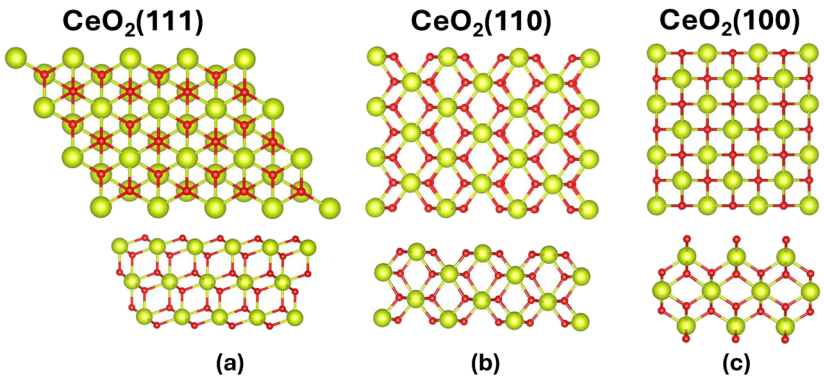

FIG. 1. Top (above) and side (below) views of the three low-index surfaces of CeO_2: (a) $CeO_2(111)$, (b) $CeO_2(110)$, and (c) $CeO_2(100)$. Color code: cerium: green and oxygen: red.

positioned between two Ce^{4+} ions of the first layer and two oxygen O^{2-} ions of the second layer, predicting a redshifted CO harmonic frequency.[63,64] Later studies also within the embedded cluster framework obtained for CO bound to the Ce^{4+} ion a blueshifted peak (+9 cm^{-1}) when employing the hybrid functional B3LYP, while when using the GGA functional PW91, the shift went to the red (−5 cm^{-1}).[65] A more recent investigation based on periodic DFT assigned the experimental band at 2170 cm^{-1} to CO bound to Ce^{4+} cations[49,51] and the weaker positive peak at 2160 cm^{-1} to two notably tilted configurations, the so-called tilt-1 and tilt-2 configurations.[51] In the first, tilt-1, the CO molecule is between a Ce^{4+} ion of the first layer and another Ce^{4+} ion of the second layer, pointing the oxygen atom of CO to the second layer Ce^{4+}. The second, (tilt-2), is equivalent to the most stable tilted arrangement found by Müller *et al.*,[63] i.e., the CO molecule is located between two Ce^{4+} ions in the first layer and two O^{2-} ions of the second layer.[51] This latter study also showed that the top and tilted configurations were nearly isoenergetic, with binding energy differences of 0.03 eV (2.9 kJ/mol) [PBE-U low CO coverage ($\theta = \frac{1}{4}$)] and 0.02 eV (1.9 kJ/mol) [HSE06 low CO coverage ($\theta = \frac{1}{4}$)], with the tilted CO arrangement being slightly more stable. In Refs. 19, 54, and 110, the formation of strongly bound carbonate CO_3^{2-}-like species has also been reported, resulting in a reduction of the ceria surface; however, such species have not been observed in the IRRAS experiment.[108] All configurations previously found in the literature were investigated in this work within the framework of an embedded cluster model and in the case of a low-coverage ($\theta \leq \frac{1}{4}$) scenario.

The $CeO_2(100)$ surface shows a more open structure, being genuinely polar, which results in an inherent instability and, consequently, induces surface reconstructions [Fig. 1(c)].[54,111] The first layer is constituted by oxygen atoms and the second by "non-reachable" cerium atoms [Fig. 1(c)]. The Ce:O coordination number on the uncovered surface is 6:2.[106] The CO adsorption on the $CeO_2(100)$ shows an experimental vibrational spectrum with an intense band at 2176 cm^{-1}, a shoulder at 2168 cm^{-1}, and a weaker peak at 2147 cm^{-1}.[42] Theoretical studies based on periodic DFT[51] have found two sites for the adsorption of CO. One presents in cases of low ($\theta \leq \frac{1}{4}$) and high ($\theta = 1$) coverages and where CO is found on a Ce^{4+}–Ce^{4+} bridge position. The other one is identified only in cases of high coverage ($\theta = 1$) and is much less stable where CO is on top of the Ce^{4+} ions. After exploring different CO adsorption sites employing the MP2 method and different basis sets (def2-SVP, def2-TZVPP, and def2-QZVPP) and considering that this work covers low coverage cases ($\theta \leq \frac{1}{4}$), only a CO on a Ce^{4+}–Ce^{4+} bridge position was found. Thus, the rest of this study focuses on this bridge configuration.

A. Analysis of the size of the QM cluster

In the case of rare earth oxides, the use of methods such as CCSD(T) clearly represents a computational challenge, even within the framework of the embedded cluster model. Therefore, clusters of different sizes and shapes were analyzed in order to determine the size necessary and sufficient to reach the desired accuracy. The CO harmonic stretching frequency was chosen to analyze the influence of the size and shape of the cluster used. In the case of CO adsorbed on $CeO_2(100)$, the impact of the bare surface employed as a starting point to apply the embedded cluster model, that is, PBE(1 × 1), PBE(2 × 2), HSE06(1 × 1), and HSE06(2 × 2), was also studied. For this aim, the MP2 method and the def2-SVP, def2-TZVPP, and def2-QZVPP basis sets have been utilized in all the cases discussed here. Regarding the structural parameters to be optimized, only the structure and position of the CO molecule were relaxed, while the surfaces were kept with the starting structures obtained by periodic DFT. This criterion regarding the relaxation of structural parameters was adopted based on the results reported for $CO@CeO_2(111)$,[62] showing that the difference in CO frequency is only about 2 cm^{-1} when surface relaxation effects are included.

1. CO on $CeO_2(100)$

For the $CeO_2(100)$ surface with CO adsorbed on a Ce^{4+}–Ce^{4+} bridge configuration, three clusters of different size and shape were designed, i.e., cluster 1 $[Ce_2O_{11}Ti_{12}]^{34+}$, cluster 2 $[Ce_4O_{20}Ti_{18}]^{48+}$, and cluster 3 $[Ce_8O_{32}Ti_{26}]^{72+}$ (see Fig. 2). The boundary region represented by ECPs of Ti^{4+} (blue color) is also included in the structures. The effect of utilizing different surface structures obtained with the functionals PBE-U [(1 × 1) and (2 × 2) cell sizes] and HSE06 [(1 × 1) and (2 × 2) cell sizes] was analyzed in the case of cluster 1 ($[Ce_2O_{11}Ti_{12}]^{34+}$), obtaining that the prediction of the harmonic frequency of CO is practically independent of the surface used with differences of ≤1 cm^{-1} with values for the HSE06 (2 × 2) surface of 2180, 2148, 2155, and 2156 cm^{-1} using the basis sets def2-SVP,

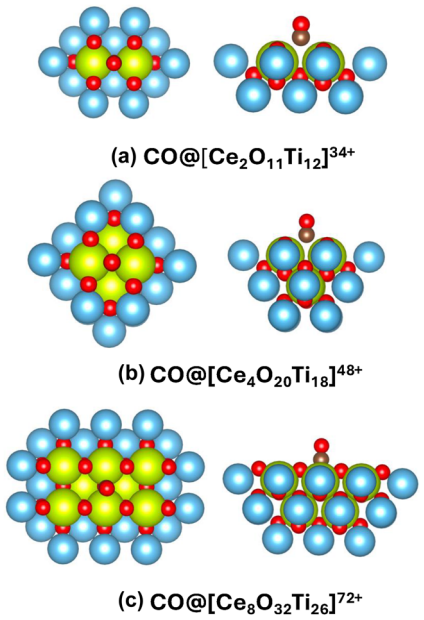

FIG. 2. Structure of the three clusters studied in this work for the $CeO_2(100)$ surface: (a) $[Ce_2O_{11}Ti_{12}]^{34+}$, (b) $[Ce_4O_{20}Ti_{18}]^{48+}$, and (c) $[Ce_8O_{32}Ti_{26}]^{72+}$. In all cases, the CO molecule is located perpendicular to the surface and in a bridge position between two Ce^{4+} ions, with the central oxygen (top view) being that of the CO molecule (cerium: green, titanium: blue, and oxygen: red).

def2-TZVPP, def2-TZ/QZVPP, and def2-QZVPP, respectively (see the supplementary material). Def2-TZ/QZVPP denotes the use of the def2-QZVPP basis set for the CO molecule and the two Ce atoms between which CO forms the bridge, while for the rest of the QM cluster, the def2-TZVPP basis is utilized. At this point, it is worth mentioning that, while the results obtained with def2-SVP are unreliable, those with the def2-TZVPP and def2-TZ/QZVPP basis sets differ only by 8 and 1 cm^{-1}, respectively, from those obtained with the def2-QZVPP basis set. Based on these results, the influence of the cluster size will be analyzed only with the surface structure obtained with the screened range-separated hybrid HSE06 functional (2 × 2 cell size), whose superior performance has also been proved several times in Refs. 112 and 113. The influence of cluster size and basis sets is summarized in Fig. 3(a). It can be concluded that the cluster size has a negligible influence (~2 cm^{-1}) on the prediction of the CO frequency, even smaller than that observed in the case of CO adsorbed on $CeO_2(111)$.[62] In view of these results, the use of cluster 1 for the prediction of the CO vibrational frequency using the CCSD(T) method seems to be justified, which means that, assuming a similar behavior to that observed with the MP2 method, an overestimation of no more than 2 cm^{-1} is to be expected.

2. CO on $CeO_2(110)$

To investigate the CO configuration on top of the Ce^{4+} ions of the $CeO_2(110)$ surface, three clusters were constructed from the bare optimized surface obtained with the HSE06 functional (2 × 2 cell size) and taken from Ref. 51 [see Fig. 4(a)]. These three clusters are cluster 1a $[CeO_6Ti_9]^{28+}$, cluster 2a $[Ce_3O_{14}Ti_{19}]^{60+}$, and cluster 3a

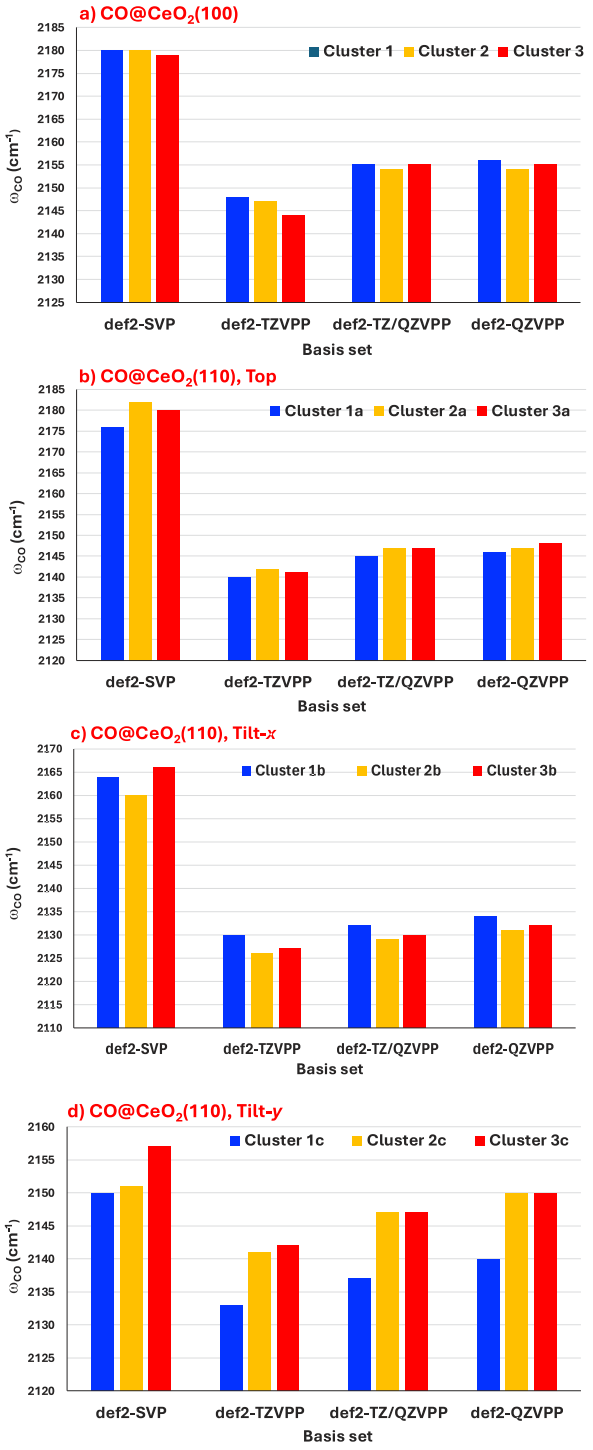

FIG. 3. CO harmonic vibrational frequency calculated with the fc-MP2 method and bare surfaces optimized using the HSE06 functional [(2 × 2) cell size].[51] Cluster size and shape dependence analysis considering only the relaxation of the CO bond length and its relative position with respect to the surface. CO adsorbed on $CeO_2(100)$ in bridge configuration (a). CO adsorbed on $CeO_2(110)$ on top (b), tilt-x (c), and tilt-y (d) configurations.

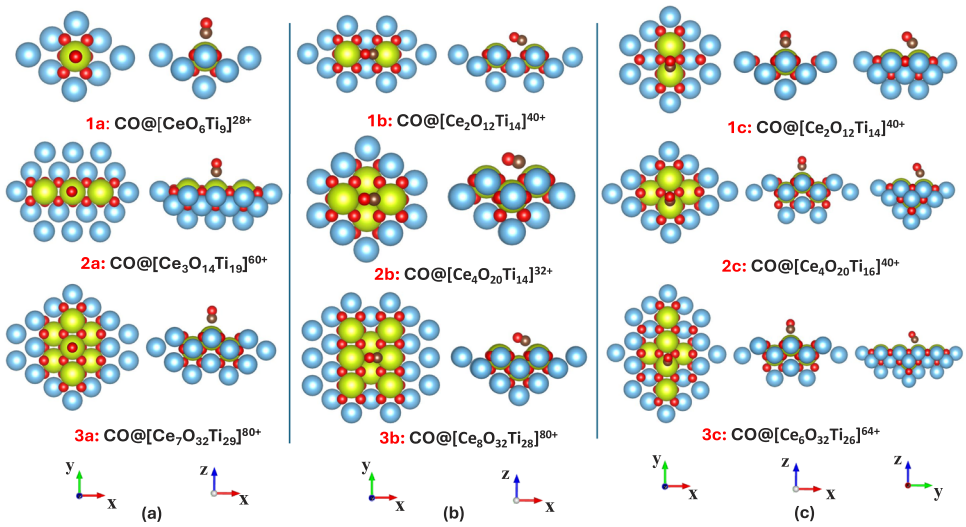

FIG. 4. Structure of the clusters studied in this work for the $CeO_2(110)$ surface: Top (a), tilt-*x* (b), and tilt-*y* (c) sites. In all cases, the CO is included in the corresponding configuration (cerium: green, titanium: blue, and oxygen: red).

$[Ce_7O_{33}Ti_{29}]^{80+}$, which already include the boundary region defined by ECPs of Ti^{4+} (blue color). In this case, the def2-TZ/QZVPP basis set employs the def2-QZVPP basis set for CO and the Ce atom directly interacting with the CO molecule and the def2-TZVPP basis set for the rest of the QM cluster. As shown in Fig. 3(b), it can be stated that the trend is very similar to that observed at the $CeO_2(100)$ surface. The def2-SVP basis set overestimates the predicted CO frequencies by about 35 cm^{-1}, while the def2-TZVPP and def2-TZ/QZVPP basis sets differ by approximately 5–7 cm^{-1} and at most 1 cm^{-1}, respectively, from the value calculated with the def2-QZVPP basis set. With reference to the influence of the cluster size, it is observed [Fig. 3(b)] that the differences among the three clusters decrease as the size of the basis set increases; the differences between cluster 1a and cluster 3a are 4, 1, 2, and 2 cm^{-1} with the def2-SVP, def2-TZVPP, def2-TZ/QZVPP, and def2-QZVPP basis sets, respectively. Thus, cluster 1a was further used for the CCSD(T) computations. In addition, in all cases, two negative frequencies were systematically obtained and associated with two normal coordinates characterized by a bending—and slightly translational—motion of the CO molecule in the *x* and *y* directions (see Fig. 5), respectively. In principle, one could assume that these negative frequencies are due to structural constraints, since the surface remained fixed. However, the relaxation of surface parameters such as the coordinates of the Ce atom aligned to the CO molecule, as well as the four surrounding oxygen atoms of the surface, does not change this behavior.

In order to find an absolute minimum, tilted configurations along these two coordinates were investigated following the same scheme employed with the (100) and (111)[62] surfaces. Thus, Figs. 4(b) and 4(c) display the clusters that were designed to study the tilted configurations in the *x* and *y* directions, respectively. The resulting tilt-*x* configuration resembles the tilt-2 site reported by Lustemberg *et al.*,[51] which also coincides with one previously published using the embedded model[63,65] (O_4-*site*). The tilted configuration in the *y* direction (tilt-*y*) leads to a slightly tilted position

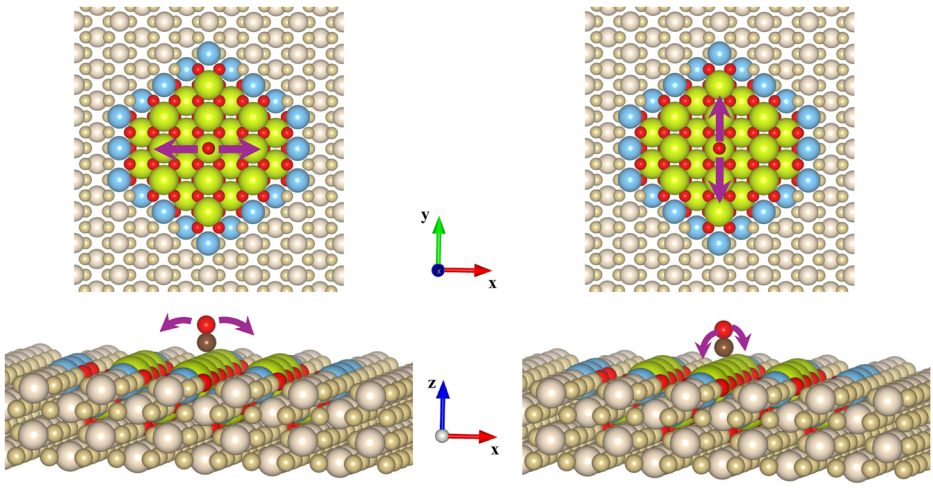

FIG. 5. Illustration of the two explored directions for the relaxation of the top position of the CO molecule adsorbed on $CeO_2(110)$ (cerium: green, titanium: blue, and oxygen: red).

of CO aligned to the Ce^{4+} ion, which can be identified with the Ce_1-*site* obtained by Hermansson *et al.*[63,65] The tilt-*x* configuration was studied, meaning three different clusters: cluster 1b $[Ce_2O_{12}Ti_{14}]^{40+}$, cluster 2b $[Ce_4O_{20}Ti_{14}]^{32+}$, and cluster 3b $[Ce_8O_{32}Ti_{28}]^{80+}$. The convergence of the cluster size and shape was analyzed through the prediction of the harmonic stretching frequency of CO using the MP2 method and four distinct basis sets; see Fig. 3(c). The trend is similar to that reported for the (100) surface and the top site of the (110) surface. The def2-SVP basis set overestimates the CO stretching frequency by 30–35 cm^{-1}. Compared with the def2-QZVPP basis set, the def2-TZVPP and def2-TZ/QZVPP basis sets underestimate the CO frequency by 5 and 2 cm^{-1}, respectively. Concerning the difference between cluster 1b and cluster 3b, this amounts to 2, 3, 2, and 2 cm^{-1} with the def2-SVP, def2-TZVPP, def2-TZ/QZVPP, and def2-QZVPP basis sets, respectively. Thus, cluster 1b was chosen to carry out the CCSD(T) computations. Following the same procedure for the tilt-*y* configuration, three clusters were constructed: cluster 1c $[Ce_2O_{12}Ti_{14}]^{40+}$, cluster 2c $[Ce_4O_{20}Ti_{16}]^{40+}$, and cluster 3c $[Ce_6O_{32}Ti_{26}]^{64+}$ (see Fig. 4). As shown in Fig. 3(d), first, it should be noted that the def2-SVP basis set overestimates the CO frequency, although not as markedly as in the previous cases [Figs. 3(a)–3(c)]. This is because it converges to structures where the CO molecule is more tilted than with larger basis sets, i.e., 30°, 28°, and 28° with respect to the surface normal, for clusters 1c, 2c, and 3c, respectively. This tilt leads to lower CO frequencies, compensating for the natural tendency of this basis to overestimate the harmonic frequency. It is also worth mentioning that in this case and for the smallest cluster, cluster 1c, the basis sets def2-TZVPP, def2-TZ/QZVPP, and def2-QZVPP predict the harmonic CO stretching frequency on the order of 10–20 cm^{-1} lower than the other two clusters and report tilt angles of 20° and contrasting with that of clusters 2c and 3c, for which the tilt angles range between 13° and 15° (def2-TZVPP and def2-TZ/QZVPP basis sets) and 0° (def2-QZVPP). Cluster 1c turns out to lead to misleading results, while clusters 2c and 3c conclude in similar frequencies and tilt angles with differences of no more than 1 cm^{-1} and 1°, respectively.

B. CO vibrational frequency

The computed CO harmonic stretching frequency of CO adsorbed on the low-index surfaces [(100), (110), and (111)] of CeO_2, calculated with the MP2 and CCSD(T) methods in conjunction with different basis sets, is presented in Table I. In all cases, the optimized bare surfaces obtained by periodic HSE06 calculations (2 × 2 cell size)[51] were used.

1. Bridge configuration of CO on CeO_2(100)

For the (100) surface and comparing the predictions made with the MP2 method with those obtained with the CCSD(T) method, it is observed that MP2 systematically underestimates the CO frequency by 52–62 cm^{-1}. With regard to the basis set convergence, the def2-SVP basis set predicts the CO harmonic frequency to be 32 and 25 cm^{-1} larger than the def2-TZVPP basis set employing the MP2 and CCSD(T) methods, respectively. With the def2-TZVPP basis set, the same frequency is 7 cm^{-1} (MP2) and 10 cm^{-1} [CCSD(T)] lower than with the def2-TZ/QZVPP basis set.

2. Top and tilted configurations of CO on CeO_2(110)

The harmonic stretching frequencies of CO on CeO_2(110) with top and tilt-*x* configurations are underestimated by 36–44 cm^{-1} and 25–30 cm^{-1}, respectively, with the MP2 method in comparison with

TABLE I. Harmonic CO stretching frequencies (in cm^{-1}) on CeO_2(100) cluster 1 $CO@[Ce_2O_{11}Ti_{12}]^{34+}$ and CeO_2(110) cluster 1a $CO@[CeO_6Ti_9]^{28+}$, cluster 1b $CO@[Ce_2O_{12}Ti_{14}]^{40+}$, and cluster 2c $CO@[Ce_4O_{20}Ti_{16}]^{40+}$ obtained using the optimized surface HSE06(2 × 2).[a]

		CeO_2(100)	CeO_2(110)			CeO_2(111)[b]
Method	Basis set	Cluster 1	Top[c] Cluster 1a	Tilt-*x* Cluster 1b	Tilt-*y* Cluster 2c[d]	Cluster 1
fc-MP2	def2-SVP	2180	2176	2164	2151 (28°)	2166
	def2-TZVPP	2148	2140	2130	2141 (14°)	2140
	def2-TZ/QZVPP	2155	2145	2132	2147 (15°)	2148
	def2-QZVPP	2156	2146	2134	⋯	2148
fc-CCSD(T)	def2-SVP	2232	2212	2189	⋯	2200
	def2-TZVPP	2207	2179	2158	⋯	2179
	def2-TZ/QZVPP	2217	2189	2164	⋯	2190

[a]In the case of the (100) site, the designation def2-TZ/QZVPP refers to the use of the def2-QZVPP basis set for the CO molecule and the two Ce atoms between which CO forms the bridge, while for the rest of the QM, the def2-TZVPP basis is utilized. For the top configuration, the (110) surface refers to the use of the def2-QZVPP basis set for CO and the Ce atom directly interacting with the CO molecule and of the def2-TZVPP basis set for the rest of the QM cluster. In the case of the tilt-*x* configuration, the def2-QZVPP basis set was employed for the CO molecule and the two Ce atoms near it, while for the rest of the system, the def2-TZVPP basis set was utilized.
[b]Reference 62. Cluster 1 was defined as $CO@[CeO_7Ti_{12}]^{38+}$.
[c]Refer to a configuration perpendicular or nearly perpendicular to the surface (see the text for more details).
[d]Values in parentheses indicate the tilt angle of the CO molecule with respect to the normal of the CeO_2(110) surface.

CCSD(T). The largest underestimations amount to 44 cm^{-1} (top) and 30 cm^{-1} (tilt-*x*) and are obtained with the def2-TZ/QZVPP basis set. Comparing the top and tilt-*x* configurations, it is observed that the harmonic CO stretching frequency in the former is of the order of 10–13 cm^{-1} (MP2) and 23–25 cm^{-2} [CCSD(T)] larger than in the latter (see Table I). While this MP2 difference agrees well with the experimental $\Delta\nu$ (10 cm^{-1}), the CCSD(T) data predict a difference about 10 cm^{-1} larger. Of course, this evaluation assumes that the anharmonic contribution is the same for both configurations. Finally, for the tilt-*y*, position the data reported in Table I are those obtained for cluster 2c (see Secs. III A 1 and III A 2). As can be seen, a tilt angle of 15° or less leads to results similar to those of the top configuration. Because of the prohibitive computational cost due to a cluster with four Ce atoms, CCSD(T) calculations for cluster 2c were not carried out in the present work. The previously described MP2 vs CCSD(T) behavior and basis set trend has also been observed for the $CO@CeO_2(111)$ system.[62] As is now the case, the latter study also pointed out that the Karlsruhe basis set def2-SVP tends to overestimate the harmonic frequencies much more than its correlation-consistent counterpart (cc-pVDZ).[114] Moreover, it was concluded that with the def2-QZVPP basis set, the results could be considered converged with an underestimation of ~5 cm^{-1} due to the non-inclusion of contributions such as relativistic effects and higher-order coupled-cluster corrections. In contrast, core–valence corrections showed no effect on the frequency shift between CO@cluster and gas-phase CO.[62] For example, for CO adsorbed on CeO_2 (110) (top configuration), the core–valence correction (ae–fc) effects for cluster 1b and $CO_{(gas)}$ amount to 4 and 3 cm^{-1}, respectively, using the cc-pwCVDZ/cc-pwCVDZ-X2C basis set, while employing the cc-pwCVTZ/cc-pwCVTZ-X2C basis set adds up to 9 cm^{-1} in both cases.

At this point and in the case of $CO@CeO_2(110)$, where different configurations are possible, it is interesting to study the influence of diffuse functions. MP2 calculations were carried out for cluster 1a (top) and cluster 1b (tilt-x) using the def2-SVPD, def2-TZVPPD, and def2-QZVPPD basis sets. For the CO harmonic vibrational frequency and the top configuration, the inclusion of diffuse functions results in differences of −10, −2, and +4 cm^{-1} in comparison to the def2-SVP, def2-TZVPP, and def2-QZVPP basis sets, respectively. For the tilt-*x* configuration, these differences are −16 cm^{-1} (def2-SVP), −7 cm^{-1} (def2-TZVPP), and −2 cm^{-1} (def2-QZVPP), respectively. From these results, it can be deduced that as the basis set becomes larger, the effect of diffuse basis functions becomes almost negligible.

Furthermore, and independently of the evaluation of the binding energies discussed in Sec. III C, a qualitative study of the relative stability of the three CO configurations on the $CeO_2(110)$ surface was also carried out. Cluster 3a $[CO@Ce_7O_{31}Ti_{24}]^{62+}$ (see Fig. 4) was used to optimize the three configurations using the MP2/def2-TZVPP level of theory (see Fig. 6). First, the tilt-*x* configuration is found to be the most stable, while the top and tilt-*y* configurations are nearly isoenergetic. These results are consistent, first, with the fact that the configuration with CO on top of the Ce^{4+} ions and perpendicular to the surface appears to be a transition state (see Sec. III A 2); second, with the fact that previous periodic DFT studies[49,51,53] identified a "nearly perpendicular" top configuration; and third, with the possibility that the three configurations coexist experimentally, since the energy difference is only

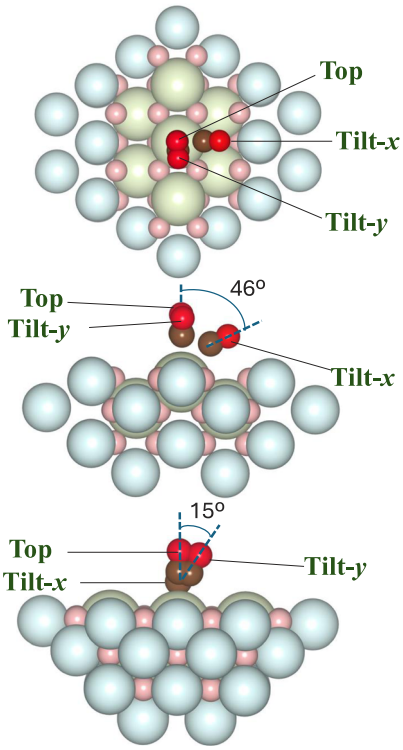

	Tilt-*x*	Top	Tilt-*y*
ΔE/ eV	0	0.040	0.037
Δω/ cm^{-1}	0	> +10	> +10

FIG. 6. Structure of the three CO configurations studied in this work for the $CeO_2(110)$ using the cluster 3a $[Ce_7O_{32}Ti_{29}]^{80+}$ and employing the MP2/def2-TZVPP level of theory. Color code: cerium: green, titanium: blue, and oxygen: red. For the surface atoms, faded colors were chosen to highlight the CO positions.

of the order of 3.9 kJ/mol. Regarding the CO harmonic vibrational frequency, it is confirmed that for both the top and tilt-*y* cases, the frequency values are higher than the tilt-*x*, although the shifts can only be considered qualitative at this level of theory. In order to further explore the influence of the CO position on the potential energy surface (PES) and on the CO frequency shift between different CO configurations, the qualitative study with cluster 3 was extended to survey the tilt-*x* configuration along the *xy* plane and the top/tilt-*y* configurations along the *yz* plane (see Fig. 7), the central Ce atom of the cluster always being the rotation center. In both cases, a 90° rotation was performed in increments of 10°; in each, only the CO distance was relaxed, keeping the position of the CO molecule fixed with respect to the *z* and *x* axes for the tilt-*x* and top/tilt-*y* configurations, respectively. From the information collected in Fig. 7, it can be deduced that in the case of the tilt-*x* configuration, the rotation around the *z* axis leads to progressively more unstable configurations and to more redshifted frequencies. Nevertheless, the configurations at 10°, 20°, and 30° are only 1.0, 3.9, and 6.7 kJ/mol less stable than the tilt-*x* configuration, respectively, which means they may coexist under experimental conditions (T = 75 K). In fact,

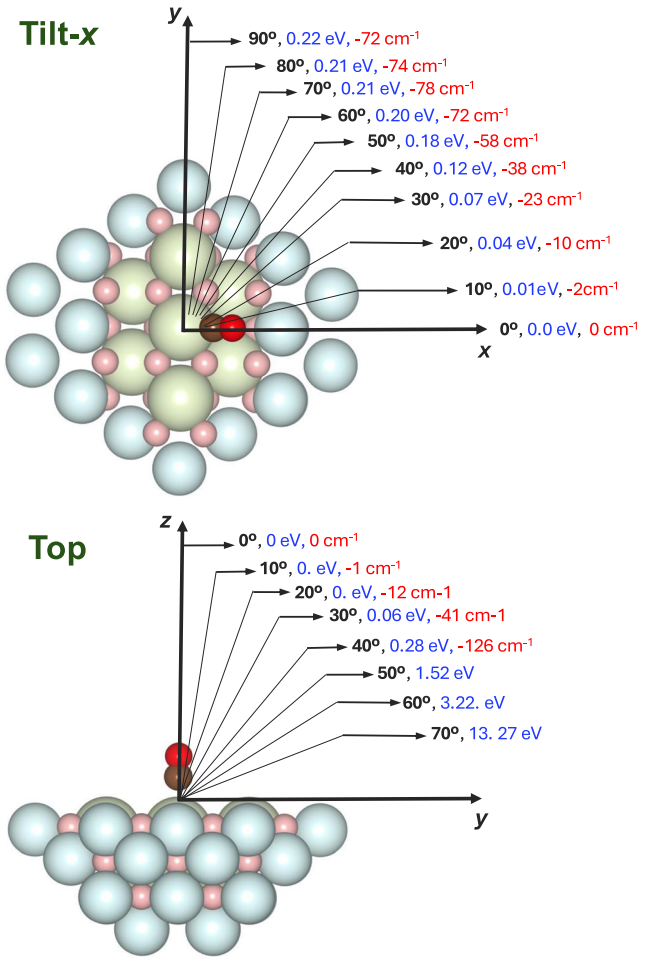

FIG. 7. Movement of the CO molecule along the *xy* plane (tilt-*x* configuration) and *zy* plane (top configuration) using cluster 3a $[Ce_7O_{32}Ti_{29}]^{80+}$ and considering as rotation center the central Ce atom. Color code: cerium: green, titanium: blue, and oxygen: red. For the surface atoms, faded colors were chosen to highlight the CO positions.

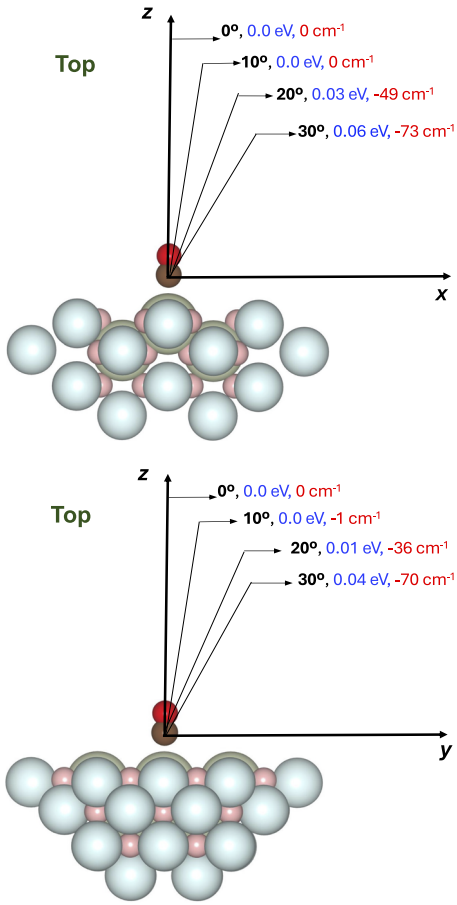

FIG. 8. Movement of the CO molecule in top configuration along the *zx* and *zy* planes using cluster 3a $[Ce_7O_{32}Ti_{29}]^{80+}$ and considering as rotation center the carbon atom. Color code: cerium: green, titanium: blue, and oxygen: red. For the surface atoms, faded colors were chosen to highlight the CO positions.

the 20° position resembles the tilt-1 configuration identified by Lustemberg *et al.*[51] using periodic DFT. With respect to the top/tilt-y configurations and the CO displacement along the *yz* plane, it can be confirmed that below ~15°, the energy difference is completely negligible and that these configurations under experimental conditions would be potentially feasible. It is again observed that the more the molecule is tilted, the more the CO harmonic frequency experiences a significant red shift that amounts to a range between 10 and 30 cm^{-1}. The tilt movement of CO from the top position, but taking this time the carbon atom as the center of coordinates, was also qualitatively (MP2/def2-TZVPP level of theory) explored along the *xy* and *yz* planes; see Fig. 8. While energy and harmonic CO frequency essentially do not change for slopes below ~15° and 10°, configurations at 20° and 30° along the *xz* and *yz* axes, respectively, are only 3–6 kJ/mol and 1–4 kJ/mol less stable than the top configuration, also showing CO frequencies between 50 and 75 cm^{-1} redshifted. It can be concluded that, starting from the tilt-*x* configuration, other nearly isoenergetic configurations would be possible within a radius of about 20°–30° in the *xy* plane. Similar observations occur in the case of the top/tilt-y configuration defined along the *yz* plane. In addition, for the CO top position itself, there exists a 10°–15° tilt-cone of possible configurations that could occur under experimental conditions and that result in small redshifted CO frequencies. These facts describe a case of multiple configurational dynamics, in which, at least in the low-coverage case ($\theta \leq \frac{1}{4}$), various CO configurations could be present experimentally.

3. Anharmonic contribution

Improvements beyond the results obtained so far involve the incorporation of anharmonic effects into the harmonic frequencies calculated at different levels of theory. Considering the weakly bound nature of CO and its rather small anharmonic nature, the anharmonic contribution was estimated using an approach that

combines a Finite Basis Representation (FBR) with a Discrete Variable Representation (DVR) of the potential energy based on vibrational normal coordinates and in conjunction with an analytic form of the kinetic energy operator.[104] While the method-dependent factor,[49,51,115] usually employed in theoretical catalysis, simultaneously corrects the limitations of a specific DFT functional and the lack of anharmonic corrections, the procedure followed here takes only the anharmonic contribution into account. The values obtained in this research are presented in Table II. As for the system $CO@CeO_2(111)$, the anharmonic corrections amount to about 25–26 cm^{-1} regardless of the method and basis set used. As already mentioned in our previous work on $CO@CeO_2(111)$,[62] this value is close to the experimental anharmonicity of the CO molecule (26.5716 cm^{-1}),[109] which again confirms the weakly bound character of CO on the three low-index surfaces of CeO_2. Analyzing the data presented in Table II, it is observed that the best theoretical estimates obtained at the CCSD(T)/def2-TZ/QZVPP level of theory for the three low-index CeO_2 surfaces contrast differently with the experimental data. While the data for the (111) and (100) surfaces estimate the CO frequencies 12 and 17 cm^{-1} above the experimental value, respectively, in the case of the (110) surface, the predicted frequencies are somewhat below the experimental data, in particular 7 cm^{-1} (top) and 21 cm^{-1} (tilt-*x*) below the negative and positive experimental features, respectively. At this point, it should be stressed again that this study focuses only on the low coverage case ($\theta \leq \frac{1}{4}$), while the experimental data all come from a coverage saturation of 1 ML. Studies based on periodic DFT and using the HSE06 functional compared the CO frequency in the high ($\theta = 1$, i.e., 1 ML saturation) and low coverage cases ($\theta \leq \frac{1}{4}$) and arrived at the conclusions that in the case of the (111) and (100) surfaces, high coverage results in a redshift of about −4 and −8 cm^{-1}, respectively, while in the case of the (110) surface, high coverage means a redshift of only −1 cm^{-1} (top configuration) and a blueshift of about +4 cm^{-1} (tilt-x configuration).[51] Taking into account these corrections on the low coverage predictions made in this work, the differences with the experimental data would become +8, +9, −8, and −17 cm^{-1} for the (111), (100), (110) (top), and (110) (tilt-*x*) surfaces, respectively. To this outcome, it needs to be added that the methodology applied here assumes an uncertainty of ±5 cm^{-1} already established in our previous work.[62] According to what was previously discussed, a multi-configurational character is identified in the adsorption of CO on the (110) surface, especially for tilted positions, which is clearly poorly described through only one configuration (tilt-x). In addition, it should be asserted that a high coverage scenario is expected to modify these multi-configurational dynamics to some extent, since the interaction between different CO molecules adsorbed on the surface will alter the PES and vibrational spectrum of this system.

C. CO binding energy on the $CeO_2(100)$ and $CeO_2(110)$ surfaces

The adsorption energy of CO adsorbed on the low-index surfaces of ceria was calculated according to the following formula:

$$E_{ads} = E[CO@CeO_2(\alpha\beta\gamma)] - E[CeO_2(\alpha\beta\gamma)] - E[CO_{gas}], \quad (1)$$

where $E[CeO_2(\alpha\beta\gamma)]$, $E[CeO_2\ (\alpha\beta\gamma)]$, and $E[CO_{gas}]$ represent the energy of the (100) and (110) surfaces with the adsorbed CO molecule (i.e., one of the embedded clusters; see Figs. 2 and 4), the energy of the (100) and (110) surfaces without adsorbate (i.e., embedded clusters without CO adsorbed), and the energy of the

TABLE II. Computed anharmonic CO stretching frequencies (in cm^{-1}) for cluster 1: $CO@[Ce_2O_{11}Ti_{12}]^{34+}$ of $CeO_2(100)$ and cluster 1a: $CO@[CeO_6Ti_9]^{28+}$ and cluster 1b: $CO@[Ce_2O_{12}Ti_{14}]^{40+}$ of $CeO_2(110)$ obtained using the bare surface HSE06(2 × 2). The data in parentheses and italics correspond to the anharmonic correction (in cm^{-1}).[a]

		$CeO_2(100)$	$CeO_2(110)$		$CeO_2(111)$[b]
Method	Basis set	Cluster 1	Top[c] Cluster 1a	Tilt-*x* Cluster 1b	Cluster 1
fc-MP2	def2-SVP	2154(*−26*)	2151(*−25*)	2139 (*−26*)	2142(*−24*)
	def2-TZVPP	2122(*−26*)	2114(*−26*)	2104 (*−25*)	2115(*−25*)
	def2-TZ/QZVPP	2129(*−26*)	2120(*−26*)	2107 (*−25*)	2123(*−25*)
	def2-QZVPP	2129(*−27*)	2120 (*−26*)	2108 (*−26*)	2123(*−25*)
fc-CCSD(T)	def2-SVP	2207(*−25*)	2187(*−25*	2163 (*−26*)	2176(*−25*)
	def2-TZVPP	2181(*−26*)	2153(*−25*)	2133(*−25*)	2154(*−25*)
	def2-TZ/QZVPP	2193(*−25*)	2163(*−25*)	2139 (*−25*)	2166(*−25*)
Exp.[d]		2176, 2168_{sh}[e]	2170, 2160		2154

[a]In the case of the (100) site, the designation def2-TZ/QZVPP refers to the use of the def2-QZVPP basis set for the CO molecule and the two Ce atoms between which CO forms the bridge, while for the rest of the QM, the def2-TZVPP basis is utilized. For the top configuration, the (110) surface refers to the use of the def2-QZVPP basis set for CO and the Ce atom directly interacting with the CO molecule and of the def2-TZVPP basis set for the rest of the QM cluster. In the case of the tilt-*x* configuration, the def2-QZVPP basis set was employed for the CO molecule and the two Ce atoms near it, while for the rest of the system, the def2-TZVPP basis set was utilized.
[b]Reference 62. Cluster 1 refers to $CO@[CeO_7Ti_{12}]^{38+}$.
[c]It refers to a configuration perpendicular or nearly perpendicular to the surface (see the text for more details).
[d]Polarization-resolved IRRAS experiment of 1 monolayer (ML) CO adsorbed on oxidized $CeO_2(100)$ and $CeO_2(110)$ single-crystal surfaces at low temperatures (70 K). References 42, 107, and 108.
[e]"sh" denotes the *shoulder*.

CO molecule in the gas phase, respectively. Because of the basis-set incompleteness, this expression for the adsorption energy was approximately corrected for the basis-set superposition error (BSSE) employing the full counterpoise (CP)[116] scheme. This means that the final binding energy is given by

$$E_{ads+CP} = E_{ads} + \Delta E[CeO_2(\alpha\beta\gamma)] + \Delta E[CO] \quad (2)$$

being

$$\Delta E[CeO_2(\alpha\beta\gamma)] = E[CeO_2(\alpha\beta\gamma)] - E_{ghost}[CeO_2(\alpha\beta\gamma)]_{[CO@CeO_2(\alpha\beta\gamma)]} \quad (3)$$

and

$$\Delta E[CO] = E[CO] - E_{ghost}[CO]_{[CO@CeO_2(\alpha\beta\gamma)]}. \quad (4)$$

Equations (3) and (4) represent the fragment energies at the same coordinates as in the embedded cluster with adsorbate [i.e., $CO@CeO_2(\alpha\beta\gamma)$] and using the basis set for the whole system, in other words, a "ghost" basis for the missing fragment. Only the relaxation of the CO molecule was considered. The contribution coming from the harmonic vibrational zero-point energy (ZPE) includes only the 3N (N = 2) vibrational degrees of freedom of the CO molecule adsorbed on the surface as well as the 3N-5 vibrational degrees of freedom of the free CO. Values for cluster 1 ($CO@[Ce_2O_{11}Ti_{12}]^{34+}$) for $CeO_2(100)$ and clusters 1a ($CO@[CeO_6Ti_9]^{28+}$) and 1b ($CO@[Ce_2O_{11}Ti_{12}]^{34+}$) for the top and tilt-$x$ configurations, respectively, for $CeO_2(110)$ are reported in Table III, including data with (wCP) and without (woCP) counterpoise correction (CP), ZPE corrections, and relaxation of the CO molecule. It is important to mention that the CP correction has an approximate character, typically converging only at the complete basis set (CBS) limit.[118] Thus, multiple studies have proposed the use of only half of the CP correction, expecting that the most plausible values for the binding energy will lie between the data with and without the CP contribution.[119–121] According to the results of our previous study on $CO@CeO_2(111)$, the cluster size does not have a relevant influence on the binding energy values.[62] Thus, in the present work, this physical magnitude was evaluated only on the clusters in which the most detailed analysis of the CO vibrational frequency was made, that is, those that appear in Tables I and II. The results obtained for the (100) and (110) surfaces, as well as those for the (111) surface,[62] using the same methodology as the one applied in this research, are presented in Table III. Additional data from

TABLE III. CO adsorption energy (E_{ads} in eV) for cluster 1 ($CO@[Ce_2O_{11}Ti_{12}]^{34+}$) for $CeO_2(100)$ and cluster 1a ($CO@[CeO_6Ti_9]^{28+}$) and 1b ($CO@[Ce_2O_{11}Ti_{12}]^{34+}$) for the top and tilt-$x$ configurations, respectively, of $CeO_2(110)$ obtained using the optimized HSE06(2 × 2) bare surfaces.[51] Literature values ($E_{ads}^{lit.}$ in eV) are also included.[a,b]

		$CeO_2(100)$		$CeO_2(110)$				$CeO_2(111)$[c]	
		Top		Top[d]		Tilt-x		Top	
Method	Basis set	woCP	wCP	woCP	wCP	woCP	wCP	woCP	wCP
fc-MP2	def2-SVP	−0.66	−0.21	−0.29	−0.06	−0.56	−0.10	−0.32	+0.06
	def2-TZVPP	−0.68	−0.44	−0.30	−0.19	−0.42	−0.23	−0.30	−0.15
	def2-TZ/QZVPP	−0.68	−0.49	−0.33	−0.21	−0.49	−0.22	−0.35	−0.17
	def2-QZVPP	−0.68	−0.49	−0.28	−0.22	−0.39	−0.25	−0.30	−0.19
fc-CCSD(T)	def2-SVP	−0.58	−0.13	−0.26	−0.03	−0.54	−0.07	−0.30	+0.08
	def2-TZVPP	−0.59	−0.35	−0.27	−0.16	−0.39	−0.19	−0.27	−0.12
	def2-TZ/QZVPP	−0.58	−0.40	−0.29	−0.17	−0.41	−0.20	−0.32	−0.14
$E_{ads}^{lit.}$		−0.29[e], −0.31[f]		−0.15[e],−0.16[f]		−0.19[e],−0.21[f]		−0.26[g],−0.28[h] −0.27[i]	

[a] *woCP* and *wCP* refer, respectively, to without and with: counterpoise correction (CP), ZPE contributions, and CO relaxation.
[b] In the case of the (100) site, the designation def2-TZ/QZVPP refers to the use of the def2-QZVPP basis set for the CO molecule and the two Ce atoms between which CO forms the bridge, while for the rest of the QM, the def2-TZVPP basis is utilized. For the top configuration, the (110) surface refers to the use of the def2-QZVPP basis set for CO and the Ce atom directly interacting with the CO molecule and of the def2-TZVPP basis set for the rest of the QM cluster. In the case of the tilt-x configuration, the def2-QZVPP basis set was employed for the CO molecule and the two Ce atoms near it, while for the rest of the system, the def2-TZVPP basis set was utilized.
[c] Data from Ref. 62.
[d] Nearly perpendicular.
[e] Reference 51. Periodic DFT using the PBE functional together with a Hubbard U-like term.
[f] Reference 51. Periodic DFT using the hybrid functional HSE06 and $\theta = \frac{1}{4}$ CO coverage.
[g] Reference 117.
[h] Reference 60.
[i] References 107 and 108.

the literature are also incorporated into the latter table. Comparing the MP2 and CCSD(T) methods, the former tends to slightly overestimate the binding energy, with values about 0.03–0.04 eV larger than the CCSD(T) results. This trend is in accord with a redshift with respect to the harmonic frequency of $CO_{(gas)}$ as well as with an underestimation of the harmonic frequency of CO in the system CO@cluster in comparison with the predictions obtained with the CCSD(T) method (see Sec. III B). Other conclusions to be drawn from Table III are the following: first, that regardless of the surface, the CP corrections account for ~50% of the contribution to the total binding energy; this behavior has also been recently observed for CO adsorption on Al_2O_3(0001);[122] second, the binding energy increases slightly with the size of the basis set; finally, based on the best estimate obtained at the CCSD(T)/def2-TZ/QZVPP level of theory, the data presented here describe a physisorption phenomenon for the adsorption of CO on the three low-index CeO_2 surfaces with binding energies in the range of −0.20 eV to −0.14 eV. In the specific case of the (110) surface and the two configurations studied in this research up to the CCSD(T) level of theory (i.e., top and tilt-*x*), the difference in binding energy amounts to 0.03 eV, with the tilt configuration being the most stable. This confirms the data in the existing literature[51] and is in line with the stability study discussed in Sec. III B 2.

The addition of diffuse functions employing the MP2 method shows for the three CO adsorption configurations analyzed in this work—CeO_2(100) (top) and CeO_2(110) (top and tilt-*x*)—a generalized increase between −0.10 and −0.05 eV of the binding energy employing the def2-SVPD, def2-TZVPPD, and def2-QZVPPD basis sets and without CP correction. The inclusion of the CP correction yields binding energies only between −0.04 and −0.02 eV larger than without diffuse functions (see the supplementary material). Thus, it can be concluded that these contributions do not alter the qualitative interpretation of the adsorption energies. Regarding the core–valence corrections, calculations carried out with the MP2 method correlating all electrons (ae) and using the correlation constant polarized *weighted* core–valence basis set (cc-pwCVnZ, n = D,T) indicate that in all cases these contributions only increase the binding energies in the order of −0.02/−0.03 eV, and it can be surmised that core–valence corrections are negligible for the adsorption energies determined in this study.

IV. SUMMARY

This work presents a systematic study of the CO adsorption on three low-index CeO_2 surfaces, i.e., (100), (110), and (111), using wave-function based methods such as MP2 and CCSD(T) in the context of an embedded cluster model. From the theoretical perspective, it is concluded that the best results were those obtained at the CCSD(T)/def2-TZ/QZVPP level of theory using CeO_2 bare surfaces periodically optimized employing the HSE06 functional [(2 × 2) cell size].[51] The best theoretical estimates for the CO frequency on the CeO_2(111) (2166 cm^{-1}) and CeO_2(100) (2193 cm^{-1}) surfaces obtained at the CCSD(T)/def2-TZ/QZVPP level of theory are 12 and 17 cm^{-1} larger than the experimental values obtained under 1 ML coverage conditions. Previous periodic DFT investigations[51] already estimated a blueshift of ~4 cm^{-1} (111) and 8 cm^{-1} (100) for low coverage conditions; then the calculated data would likely be ≈8 and ≈9 cm^{-1} larger than the experimental evidence for the CeO_2(111) and CeO_2(100) surfaces, respectively. This low coverage blueshift has also been observed previously on the frequency of CO adsorbed on MgO(001), where a shift from 2150.2 cm^{-1} (at $\theta = \frac{1}{4}$) to 2157.5 cm^{-1} (at $\theta \to 0$) was observed.[123] For this case, periodic LNO-CCSD(T)[124] computations predict, however, the CO vibrational frequency on CO@MgO(001) ($\theta \to 0$) at 2173.9 cm^{-1}, which is 16.4 cm^{-1} larger than the experimental value.[123] For the (110) surface, the theoretical and experimental data compare differently. The CCSD(T)/def2-TZ/QZVPP values are −7 cm^{-1} (top configuration) and −21 cm^{-1} (tilt-*x* configuration) lower than the two experimental features measured at 2170 cm^{-1} (negative feature) and 2160 cm^{-1} (positive feature). In this case, the high-coverage corrections were estimated to cause a redshift of 1 cm^{-1} and a blueshift of 4 cm^{-1} for the top and tilt-*x* configurations, respectively. These contributions added to our best estimates result in final values that differ from the experiment by −8 and −17 cm^{-1} for the top and tilt-*x* configurations, respectively. Moreover, in view of the presented results concerning the adsorption of CO on CeO_2(110), the basis for assigning the experimental data to only two "static" configuration figures (top and tilt) is insufficient. This alludes to the existence of a range of configurations almost perpendicular (10°–15°) to the surface and another where the molecule is clearly tilted and adopts different positions in a range of 20°–25° rotation along the *xy* plane. A similar situation was described in the case of CO@MgO(001)[125] and for CO@CeO_2(110)[51] in the context of periodic DFT under 1 ML coverage. Our best predictions (CCSD(T)/def2-TZ/QZVPP), which deviate by −5 cm^{-1} (top) and −16 cm^{-1} (tilt-*x*) from the two experimental features, are plausible. Any top configuration of CO on the low-index CeO_2 surfaces leads to a blue shift; however, the tilted configurations found on the (110) surface result in very close frequencies to the CO value in the gas phase.[51]

Regarding the binding energies, the results obtained at the CCSD(T)/def2-TZ/QZVPP level of theory indicate that the cases where CO is most weakly bound to the surface are the top positions on the (111) (−0.13 eV) and (110) (−0.17 eV) surfaces. For the (110) surface, the most stable configuration (tilt-*x*) exhibits a slightly larger binding energy of −0.20 eV (−0.03 eV more stable than the top configuration). The CO bridge position on the (100) surface results in a binding energy of −0.40 eV, which is almost twice the value of the other two surfaces. Based on these results, it can be summarized that the top configurations are those in which the CO-surface interaction is weakest, followed closely by the tilted configuration (tilt-x) on the (110) surface. Finally, the CO bridge position on the (100) surface appears to be more strongly bound to the surface; however, it is within the framework of what could be defined as a physisorption case.

Limitations of the presented approach are (1) surfaces optimized with the HSE06 functional as the best description of the bare surfaces, (2) the fact that the model is based on a low coverage case ($\theta \leq \frac{1}{4}$), (3) the no inclusion of relativistic effects and high-order coupled-cluster-corrections, and (4) the intrinsic error associated with the cluster size and shape. For the last three aspects an uncertainty of ±5 cm^{-1} is estimated for the present work, as well as for our previous study on the CeO_2(111) surface.[62]

SUPPLEMENTARY MATERIAL

The supplementary material contains information on the use of bare surfaces for $CeO_2(100)$ optimized with different functionals and supercell sizes. It also includes data on the effect of diffuse basis functions on the prediction of the CO adsorption energy on $CeO_2(100)$ (bridge), $CeO_2(110)$ (top), and $CeO_2(110)$ (tilt-x).

ACKNOWLEDGMENTS

The author acknowledges the "Virtual Materials Design" (VirtMat) initiative at the Karlsruhe Institute of Technology (KIT), funded by the Helmholtz Association and within the Joint Lab VMD, as well as the Deutsche Forschungsgemeinschaft (DFG) (German Research Foundation) through the Grant No. SFB 1441 – Project-ID: 426888090 (Subproject A4). The author also acknowledges the support by the state of Baden-Württemberg and the German Research Foundation (DFG) through the bwHPC Grant No. INST 40/575-1 FUGG (JUSTUS 2 cluster).

AUTHOR DECLARATIONS

Conflict of Interest

The authors have no conflicts to disclose.

Author Contributions

Juana Vázquez Quesada: Conceptualization (lead); Data curation (lead); Formal analysis (lead); Funding acquisition (lead); Investigation (lead); Methodology (lead); Project administration (lead); Resources (lead); Software (lead); Supervision (lead); Validation (lead); Visualization (lead); Writing – original draft (lead); Writing – review & editing (lead).

DATA AVAILABILITY

The data that support the findings of this study are available within the article and its supplementary material.

REFERENCES

[1]C. Yang, H. Idriss, Y. Wang, and C. Wöll, "Surface structure and chemistry of CeO_2 powder catalysts determined by surface-ligand infrared spectroscopy (SLIR)," Acc. Chem. Res. **57**, 3316 (2024).

[2]C. Yang and C. Wöll, "Infrared reflection-absorption spectroscopy (IRRAS) applied to oxides: Ceria as a case study," Surf. Sci. **749**, 122550 (2024).

[3]B. Zerulla, M. Krstić, S. Chen, Z. Yu, D. Beutel, C. Holzer, M. Nyman, A. Nefedov, Y. Wang, T. G. Mayerhöfer, C. Wöll, and C. Rockstuhl, "Polarization-dependent effects in vibrational absorption spectra of 2D finite-size adsorbate islands on dielectric substrates," Phys. Chem. Chem. Phys. **26**, 13683 (2024).

[4]M. Trenary, "Reflection absorption infrared spectroscopy and the structure of molecular adsorbates on metal surfaces," Annu. Rev. Phys. Chem. **51**, 381 (2000).

[5]L. Caulfield, E. Sauter, H. Idriss, Y. Wang, and C. Wöll, "Bridging the pressure and materials gap in heterogeneous catalysis: A combined UHV, *in situ*, and operando study using infrared spectroscopy," J. Phys. Chem. C **127**, 14023 (2023).

[6]G. Pacchioni, "Quantum chemistry of oxide surfaces: From CO chemisorption to the identification of the structure and nature of point defects on MgO," Surf. Rev. Lett. **07**, 277 (2000).

[7]C. Wöll, "Structure and chemical properties of oxide nanoparticles determined by surface-lingand IR spectroscopy," ACS Catal. **10**, 168 (2020).

[8]N. W. Ashcroft and N. D. Mermin, *Solid State Physics* (Harcourt Brace College Publishers, 1999).

[9]N. López, N. Almora-Barrios, G. Carchini, P. Błoński, R. García-Muelas, G. Novell-Leruth, and M. García-Mota, "State-of-the-art and challenges in theoretical simulations of heterogeneous catalysis at the microscopic level," Catal. Sci. Technol. **2**, 2405 (2012).

[10]M. K. Sabbe, M.-F. Reyniers, and K. Reuter, "First-principles kinetic modeling in heterogeneous catalysis: An industrial perspective on best-practice, gaps and needs," Catal. Sci. Technol. **2**, 2010 (2012).

[11]T. Gruber, K. Liao, T. Tsatsoulis, F. Hummel, and A. Grüneis, "Applying the coupled-cluster ansatz to solids and surfaces in the thermodynamic limit," Phys. Rev. X **8**, 021043 (2018).

[12]I. Y. Zhang and A. Grüneis, "Coupled cluster theory in material science," Front. Mater. **6**, 123 (2019).

[13]V. A. Neufeld, H.-Z. Ye, and T. C. Berkelbach, "Ground-state properties of metallic solids from *ab initio* coupled-cluster theory," J. Phys. Chem. Lett. **13**, 7497 (2022).

[14]T. Schäfer, F. Libisch, G. Kresse, and A. Grüneis, "Local embedding of coupled cluster theory into the random phase approximation using plane waves," J. Chem. Phys. **154**, 011101 (2021).

[15]H.-Z. Ye and T. C. Berkelbach, "*Ab initio* surface chemistry with chemical accuracy: Application to water on metal oxides," arXiv:2309.14640 (2024).

[16]H.-Z. Ye and T. C. Berkelbach, "Periodic local coupled-cluster theory for insulator and metals," J. Chem. Theory Comput. **20**, 8948 (2024).

[17]A. M. Burow, M. Sierka, J. Döbler, and J. Sauer, "Point defects in CaF_2 and CeO_2 investigated by the electrostatic embedded cluster method," J. Chem. Phys. **130**, 174710 (2009).

[18]P. Huang and E. A. Carter, "Self-consistent embedding theory for locally correlated configuration interaction wave functions in condensed matter," J. Chem. Phys. **125**, 084102 (2006).

[19]P. Huang and E. A. Carter, "Advances in correlated elctronic structure methods for solids, surfaces, and nanostructures," Annu. Rev. Phys. Chem. **59**, 261 (2008).

[20]H.-H. Lin, L. Maschio, D. Kats, D. Usvyat, and T. Heine, "Fragment-based restricted active space configuration interaction with second-order corrections embedded in periodic Hartree–Fock wavefunction," J. Chem. Theory Comput. **16**, 7100 (2020).

[21]B. T. G. Lau, G. Knizia, and T. C. Berkelbach, "Reginal embedding enables high-level quantum chemistry for surface science," J. Phys. Chem. Lett. **12**, 1104 (2021).

[22]X. Wen, J.-N. Boyn, J. M. P. Martinez, Q. Zhao, and E. A. Carter, "Strategies to obtain reliable energy landscapes from embedded multireference correlated wavefunction methods for surface reaction," J. Chem. Theory Comput. **20**, 6037 (2024).

[23]Q. N. Tran, O. Gimello, N. Tanchoux, M. Ceretti, S. Albonetti, W. Paulus, B. Bonelli, and F. Di Renzo, "Transition metal B-site substitutions in $LaAlO_3$ perovskites reorient bio-ethanol conversion reactions," Catalysts **11**, 344 (2021).

[24]O. Padilla, J. Munera, J. Gallego, and A. Santamaria, "Approach to the characterization of monolithic catalysts based on la perovskite-like oxides and their application for VOC oxidation under simulated indoor environment conditions," Catalysts **12**, 168 (2022).

[25]J. Feng, X. Zhang, J. Wang, X. Ju, L. Liu, and P. Chen, "Applications of rare earth oxides in catalytic ammonia synthesis and decomposition," Catal. Sci. Technol. **11**, 6330 (2021).

[26]C. Yang, X. Yu, S. Hei, P. G. Weidler, A. Nefedov, Y. Wang, C. Wöll, T. Kropp, J. Paier, and J. Sauer, "O_2 activation on ceria catalysts—The inportance of substrate crystallographic orientation," Angew. Chem., Int. Ed. **56**, 16399 (2017).

[27]T. Montini, M. Melchionna, M. Monai, and P. Fornasiero, "Fundamentals and catalytic applications of CeO_2-based materials," Chem. Rev. **116**, 5987 (2016).

[28]J. Paier, C. Penschke, and J. Sauer, "Oxygen defects and surface chemistry of ceria: Quantum chemical studies compared to experiment," Chem. Rev. **113**, 3949 (2013).
[29]Z. Wu, M. Li, and S. H. Overbury, "On the structure dependence of CO oxidation over CeO_2 nanocrystals with well-defined surface planes," J. Catal. **285**, 61 (2012).
[30]Y. Jiang, J. B. Adams, and M. van Schilfgaarde, "Density-functional calculation of CeO_2 surfaces and prediction of effects of oxygen partial pressure and temperature on stabilities," J. Chem. Phys. **123**, 064701 (2005).
[31]N. V. Skorodumova, S. I. Simak, B. I. Lundqvist, I. A. Abrikosov, and B. Johansson, "Quantum origin of the oxygen storage capability of ceria," Phys. Rev. Lett. **89**, 166601 (2002).
[32]S. Park, J. M. Vohs, and R. J. Gorte, "Direct oxidation of hydrocarbons in a solid-oxide fuel cell," Nature **404**, 265 (2000).
[33]G. Pulido-Reyes, I. Rodea-Palomares, S. Das, T. S. Sakthivel, F. Leganes, R. Rosal, S. Seal, and F. Fernández-Piñas, "Untagling the biological effects of cerium oxide nanoparticles: The role of surface vance states," Sci. Rep. **5**, 15613 (2015).
[34]A. Trovarelli, "Catalytic properties of ceria and CeO_2-containing materials," Catal. Rev.: Sci. Eng. **38**, 439 (1996).
[35]J. Kašpar, P. Fornasiero, and M. Granziani, "Use of CeO_2-based oxides in the three-way catalysis," Catal. Today **50**, 285 (1999).
[36]J. A. Rodríguez, D. C. Grinter, Z. Liu, R. M. Palomino, and S. D. Senanayake, "Ceria-based model catalysts: Fundamental studies on the importantce of the metal-ceria interface in CO oxidation, the water-gas shift, CO_2 hydrogenation, and methane and alcohol reforming," Chem. Soc. Rev. **46**, 1824 (2017).
[37]A. Bruix and K. M. Neyman, "Modeling ceria-based nanomaterials for catalysis and related applications," Catal. Lett. **146**, 2053 (2016).
[38]E. W. McFarland and H. Metiu, "Catalysis by doped oxides," Chem. Rev. **113**, 4391 (2013).
[39]W. Song, L. Chen, L. Wan, M. Jing, and Z. Li, "The influence of doping amount on the catalytic oxidation of formaldehyde by Mn–CeO_2 mixed oxide catalyst: A combination of DFT and microkinetic study," J. Hazard. Mater. **425**, 127985 (2022).
[40]M. Xu, H. Noei, K. Fink, M. Muhler, Y. Wang, and C. Wöll, "The surface science approach for understanding reactions on oxide powders: The importance of IR spectroscopy," Angew. Chem., Int. Ed. **51**, 4731 (2012).
[41]Y. Wang and C. Wöll, "IR spectroscopic investigations of chemical and photochemical reactions on metal oxides: Bridging the materials gap," Chem. Soc. Rev. **46**, 1875 (2017).
[42]C. Yang, M. Capdevila-Cortada, C. Dong, Y. Zhou, J. Wang, X. Yu, A. Nefedov, S. Heißler, N. López, W. Shen, C. Wöll, and Y. Wang, "Surface refaceting mechanism on cubic ceria," J. Phys. Chem. Lett. **11**, 7925 (2020).
[43]C. Li, Y. Sakata, T. Arai, K. Domen, K.-i. Maruya, and T. Onishi, "Carbon monoxide and carbon dioxide adsorption on cerium oxide studied by Fourier-transform infrared spectroscopy," J. Chem. Soc., Faraday Trans. 1: Phys. Chem. Condens. Phases **85**, 929 (1989).
[44]C. Li, Y. Sakata, T. Arai, K. Domen, K.-i. Maruya, and T. Onishi, "Adsorption of carbon monoxide and carbon dioxide on cerium oxide studied by Fourier-transform infrared spectroscopy," J. Chem. Soc., Faraday Trans. 1: Phys. Chem. Condens. Phases **85**, 1451 (1989).
[45]C. Binet, M. Daturi, and J.-C. Lavalley, "IR study of polycrystalline ceria properties in oxidised and reduced states," Catal. Today **50**, 207 (1999).
[46]J. L. F. Da Silva, M. V. Ganduglia-Pirovano, J. Sauer, V. Bayer, and G. Kresse, "Hybrid functionals applied to rare-earth oxides: The example of ceria," Phys. Rev. B **75**, 045121 (2007).
[47]M. V. Ganduglia-Pirovano, A. Hofmann, and J. Sauer, "Oxygen vacancies in transition metal and rare earth oxides: Current state of understanding and remaining challenges," Surf. Sci. Rep. **62**, 219 (2007).
[48]M. V. Ganduglia-Pirovano, "The non-innocent role of cerium oxide in heterogeneous catalysis: A theoretical perspective," Catal. Today **253**, 20 (2015).
[49]P. G. Lustemberg, P. N. Plessow, Y. Wang, C. Yang, A. Nefedov, F. Studt, C. Wöll, and M. V. Ganduglia-Pirovano, "Vibrational frequencies of cerium-oxide-bound CO: A challange for conventional DFT methods," Phys. Rev. Lett. **125**, 256101 (2020).
[50]P. Pérez-Bailac, P. G. Lustemberg, and M. V. Ganduglia-Pirovano, "Facet-dependent stability of near-surface oxygen vacancies and excess charge localization at CeO_2 surfaces," J. Phys.: Condens. Matter **33**, 504003 (2021).
[51]P. G. Lustemberg, C. Yang, Y. Wang, C. Wöll, and M. V. Ganduglia-Pirovano, "Vibrational frequencies of CO bound to all three low-index cerium oxide surfaces: A consistent theoretical description of vacancy-induced changes using density functional theory," J. Chem. Phys. **159**, 034704 (2023).
[52]M. V. Ganduglia-Pirovano, A. Martínez-Arias, S. Chen, Y. Wang, and P. G. Lustemberg, "Comment on 'surface characterization of cerium oxide catalysts using deep learning with infrared spectroscopy of CO,'" Mater. Today Sustainability **26**, 100783 (2024).
[53]A. Contreras-Payares, P. G. Lustemberg, and M. V. Ganduglia-Pirovano, "Assessing vibrational frequencies of co adsorbed on cerium oxide surfaces using SCAN and r^2SCAN functionals," J. Chem. Phys. **163**, 024701 (2025).
[54]Z. Yang, T. K. Woo, and K. Hermansson, "Strong and weak adsorption of CO on CeO_2 surfaces from first principles calculations," Chem. Phys. Lett. **396**, 384 (2004).
[55]B. X. Shi, V. Kapil, A. Zen, J. Chen, A. Alavi, and A. Michaelides, "General embedded cluster protocol for accurate modeling of oxygen vacancies in metal-oxides," J. Chem. Phys. **156**, 124704 (2022).
[56]R. H. Lavroff, D. Kats, L. Maschio, N. Bogdanov, A. Alavi, A. N. Alexandrova, and D. Usvyat, "Aperiodic fragments in periodic solids: Eliminating the need for supercells and background charges in electronic structure calculations of defects," arXiv:2406.03373 (2024).
[57]A. Kubas, D. Berger, H. Oberhofer, D. Maganas, K. Reuter, and F. Neese, "Surface adsorption energetics studied with 'gold standard' wave-function-based *ab initio* methods: Small-molecule binding to TiO_2(110)," J. Phys. Chem. Lett. **7**, 4207 (2016).
[58]B. X. Shi, A. Zen, V. Kapil, P. R. Nagy, A. Grüneis, and A. Michaelides, "Many-body methods for surface chemistry come of age: Achieving consensus with experiments," J. Am. Chem. Soc. **145**, 25372 (2023).
[59]E. Voloshina and B. Paulus, "Influence of electronic correlations on the ground-state properties of cerium dioxide," J. Chem. Phys. **124**, 234711 (2006).
[60]C. Müller, B. Paulus, and K. Hermansson, "*Ab initio* calculations of CO physisorption on ceria(111)," Surf. Sci. **603**, 2619 (2009).
[61]C. Müller and K. Hermansson, "Assessment methods for embedding schemes—Ceria as an example," Surf. Sci. **603**, 3329 (2009).
[62]J. Vázquez Quesada, S. Bernart, F. Studt, Y. Wang, and K. Fink, "CO adsorption on CeO_2(111): A CCSD(T) benchmark study using an embedded-cluster model," J. Chem. Phys. **161**, 224707 (2024).
[63]C. Müller, C. Freysoldt, M. Baudin, and K. Hermansson, "An *ab initio* study of CO adsorption on ceria (110)," Chem. Phys. **318**, 180 (2005).
[64]B. Herschend, M. Baudin, and K. Hermansson, "Electronic structure of CeO_2(110) surface oxygen vacancy," Surf. Sci. **599**, 173 (2005).
[65]B. Herschend, M. Baudin, and K. Hermansson, "CO adsorption on CeO_2(110) using hybrid-DFT embedded-cluster calculations," Chem. Phys. **328**, 345 (2006).
[66]B. Herschend, M. Baudin, and K. Hermansson, "Oxygen vacancy formation for transient structures on the CeO_2(110) surface at 300 and 750 K," J. Chem. Phys. **126**, 234706 (2007).
[67]C. Müller, B. Herschend, K. Hermansson, and B. Paulus, "Application of the method of increments to the adsorption of CO on the CeO_2(110) surface," J. Chem. Phys. **128**, 214701 (2008).
[68]H. Stoll, "On the correlation energy of graphite," J. Chem. Phys. **97**, 8449 (1992).
[69]H. Stoll, "The correlation energy of crystalline silicon," Chem. Phys. Lett. **191**, 548 (1992).
[70]H. Stoll, "Correlation energy of diamond," Phys. Rev. B **46**, 6700 (1992).
[71]D. Stodt, H. Noei, C. Hättig, and Y. Wang, "A combined experimental and computational study on the adsorption and reactions of NO on ritile TiO_2," Phys. Chem. Chem. Phys. **15**, 466 (2013).
[72]A. Rushiti and C. Hättig, "Activation of molecular O_2 on $CoFe_2O_4$ (001) surfaces: An embedded cluster study," Chem. - Eur. J. **27**, 17115 (2021).
[73]M. C. Payne, M. P. Teter, D. C. Allen, T. A. Arias, and J. D. Joannopoulos, "Iterative minimization techniques for *ab initio* total-energy calculations:

Molecular dynamics and conjugate gradients," Rev. Mod. Phys. **64**, 1045 (1992).
[74]J. P. Perdew, K. Burke, and M. Ernzerhof, "Generalized gradient approximation made simple," Phys. Rev. Lett. **77**, 3865 (1996).
[75]S. L. Dudarev, G. A. Botton, S. Y. Savrasov, C. J. Humphreys, and A. P. Sutton, "Electron-energy-loss spectra and the structural stability of nickel oxide: An LSDA+U study," Phys. Rev. B **57**, 1505 (1998).
[76]J. Heyd, G. E. Scuseria, and M. Ernzerhof, "Erratum: Hybrid functionals based on a screened Coulomb potential [J. Chem. Phys. 124, 219906 (2006)]," J. Chem. Phys. **118**, 8207 (2003).
[77]A. V. Krukau, O. A. Vydrov, A. F. Izmaylov, and G. E. Scuseria, "Influence of the exchange screening parameter on the performance of screened hybrid functionals," J. Chem. Phys. **125**, 224106 (2006).
[78]D. Du, M. J. Wolf, K. Hermansson, and P. Broqvist, "Screened hybrid functionals applied to ceria: Effect of Fock exchange," Phys. Rev. B **97**, 235203 (2018).
[79]M. V. Ganduglia-Pirovano, J. L. F. Da Silva, and J. Sauer, "Density-functional calculations of the structure of near-surface oxygen vacancies and electron localization on CeO_2(111)," Phys. Rev. Lett. **102**, 026101 (2009).
[80]See http://www.turbomole.com for TURBOMOLE V 7.7.1 2017, a development of University of Karlsruhe and Forschungszentrum Karlsruhe GmbH, 1989-2007, TURBOMOLE GmbH, since 2007.
[81]C. Møller and M. S. Plesset, "Note on an approximation treatment for many-electron systems," Phys. Rev. **46**, 618 (1934).
[82]K. Raghavachari, G. W. Trucks, J. A. Pople, and M. Head-Gordon, "A fifth-order perturbation comparison of electron correlation theories," Chem. Phys. Lett. **157**, 479 (1989).
[83]F. Weigend and R. Ahlrichs, "Balanced basis sets of split valence, triple zeta valence and quadruple zeta valence quality for H to Rn: Design and assessment of accuracy," Phys. Chem. Chem. Phys. **7**, 3297 (2005).
[84]R. Gulde, P. Pollak, and F. Weigend, "Error-balanced segmented contracted basis sets of double-ζ to quadruple-ζ valence quality for the lanthanides," J. Chem. Theory Comput. **8**, 4062 (2012).
[85]D. Rappoport and F. Furche, "Property-optimzed Gaussian basis sets for molecular response calculations," J. Chem. Phys. **133**, 134105 (2010).
[86]D. Rappoport, "Property-otimized Gaussian basis sets for lanthanides," J. Chem. Phys. **155**, 124102 (2021).
[87]F. Weigend, M. Häser, P. Patzelt, and R. Ahlrichs, "RI-MP2: Optimized auxiliary basis sets and demonstration of efficiency," Chem. Phys. Lett. **294**, 143 (1998).
[88]A. Hellweg, C. Hättig, S. Höfener, and W. Klopper, "Optimized accurate auxiliary basis sets for RI-MP2 and RI-CC2 calculations for the atoms Rb to Rn," Theor. Chem. Acc. **117**, 587 (2007).
[89]J. Chmela and M. E. Harding, "Optimized auxiliary basis sets for density fitted post-Hatree–Fock calculations of lanthanoide containing molecules," Mol. Phys. **116**, 1523 (2018).
[90]G. L. Stoychev, A. A. Auer, and F. Neese, "Automatic generation of auxiliary basis sets," J. Chem. Theory Comput. **13**, 554 (2017).
[91]M. Dolg, H. Stoll, and H. Preuss, "Energy-adjusted *ab initio* pseudopotentials for the rare earth elements," J. Chem. Phys. **90**, 1730 (1989).
[92]K. A. Peterson and T. H. Dunning, Jr., "Accurate correlation consistent basis sets for molecular core-valence correlation effects: The second row atoms Al–Ar, and the first row atoms B–Ne revised," J. Chem. Phys. **117**, 10548 (2002).
[93]Q. Lu and K. A. Peterson, "Correlation consistent basis sets for lanthanides: The atoms La–Lu," J. Chem. Phys. **145**, 054111 (2016).
[94]C. Hättig, "Optimization of auxiliary basis sets for RI-MP2 and RI-CC2 calculations: Core-valence and quintuple-ζ basis sets for H to Ar and QZVPP basis set for Li to Kr," Phys. Chem. Chem. Phys. **7**, 59 (2005).
[95]V. Rokhlin, "Rapid solution of integral equations of classical potential theory," J. Comput. Phys. **60**, 187 (1985).
[96]L. Greengard, "The rapid evaluation of potential fields in particle systems," Ph.D. thesis, Department of Computer Science, Yale University, 1987.
[97]C. A. White and M. Head-Gordon, "Derivation and efficient implementation of the fast multipole method," J. Chem. Phys. **101**, 6593 (1994).
[98]C. G. Lambert, T. A. Darden, and J. A. Board, Jr., "Multipole-based algorithm for efficient calculation of forces and potentials in macroscopic periodic assemblies of particles," J. Comput. Chem. **126**, 274 (1996).
[99]K. N. Kudin and G. E. Scuseria, "A fast multipole method for periodic systems with arbitrary unit cell geometries," Chem. Phys. Lett. **283**, 61 (1998).
[100]K. N. Kudin and G. E. Scuseria, "Revisiting infinite lattice sums with the periodic fast multipole method," J. Chem. Phys. **121**, 2886 (2004).
[101]U. Wedig, Ph.D. thesis, Karlsruher Intitut für Technologie, 1986.
[102]J. Li, H. L. Liu, and J. Ladik, "Calculation of the electron distribution of the $YBa_2Cu_3O_7$ cluster using a SCF madelung potential," Chem. Phys. Lett. **230**, 414 (1994).
[103]B. Herschend, M. Baudin, and K. Hemansson, "A combined molecular dynamics+quantum mechanics method for investigation of dynamics effects on local surface structures," J. Chem. Phys. **120**, 4939 (2004).
[104]J. Vázquez, M. E. Harding, J. F. Stanton, and J. Gauss, "Vibrational energy levels via finite-basis calculations using a quasi-analytic form of the kinetic energy," J. Chem. Theory Comput. **7**, 1428 (2011).
[105]D. R. Mullins, "The surface chemistry of cerium oxide," Surf. Sci. Rep. **70**, 42 (2015).
[106]S. Dey and G. C. Dhal, "Cerium catalysts applications in carbon monoxide oxidations," Mater. Sci. Energy Technol. **3**, 6 (2020).
[107]C. Yang, L.-L. Yin, F. Bebensee, M. Buchholz, H. Sezen, S. Heissler, J. Chen, A. Nefedov, H. Idriss, X.-Q. Gong, and C. Wöll, "Chemical activity of oxygen vacancies on ceria: A combined experimental and theoretical study on CeO_2 (111)," Phys. Chem. Chem. Phys. **16**, 24165 (2014).
[108]C. Yang, X. Yu, S. Heissler, A. Nefedov, S. Colussi, J. Llorca, A. Trovarelli, Y. Wang, and C. Wöll, "Surface faceting and reconstruction of ceria nanoparticles," Angew. Chem., Int. Ed. **56**, 375 (2017).
[109]K. P. Huber and G. H. Herzberg, "Constants of diatomic molecules," in *NIST Chemistry WebBook, NIST Standard Reference Database Number 69*, edited by P. J. Linstrom and W. G. Mallard (National Institutes of Standards and Technology, Gaithersburg, MD, 2024) (last viewed 17 December 2025).
[110]M. Nolan and G. W. Watson, "The surface dependence of CO adsorption on ceria," J. Phys. Chem. B **110**, 16600 (2006).
[111]N. V. Skorodumova, M. Baudin, and K. Hermansson, "Surface properties of CeO_2 from first principles," Phys. Rev. B **69**, 075401 (2004).
[112]T. M. Henderson, J. Paier, and G. E. Scuseria, "Accurate treatment of solids with the HSE screened hybrid," Phys. Status Solidi B **248**, 767 (2011).
[113]H.-D. Saßnick and C. Cocchi, "Electronic structure of cesium-based photocathode materials from density functional theory: Performance of PBE, SCAN, and HSE06 functionals," Electron. Struct. **3**, 027001 (2021).
[114]T. H. Dunning, Jr., "Gaussian basis sets for use in correlated molecular calculations. I. The atoms boron through neon and hydorgen," J. Chem. Phys. **90**, 1007 (1989).
[115]This is a scaling process based on the experimental and calculated frequency of the CO molecule, i.e. $\lambda = \frac{\nu^{exp}_{CO_{gas}}}{\nu^{cal}_{CO_{gas}}}$ with $\nu^{exp}_{CO_{gas}} = 2143\ cm^{-1}$ and where λ is the scale factor by which the harmonic frequency calculated for CO adsorbed on the surface is multiplied.
[116]S. F. Boys and F. Bernardi, "The calculation of small molecular interactions by the differences of separte total energies. Some procedures with reduced errors," Mol. Phys. **19**, 553 (1970).
[117]M. Nolan, S. C. Parker, and G. W. Watson, "Vibrational properties of CO on ceria surfaces," Surf. Sci. **600**, L175 (2006).
[118]W. Dononelli and T. Klüner, "Analyzing the local basis set superposition error for CO adsorbed on rutile(110)," Int. J. Quantum Chem. **121**, e26428 (2021).
[119]L. A. Burns, M. S. Marshall, and C. D. Sherrill, "Comparing counterpoise-corrected, uncorrected, and averaged binding energies for benchmarking noncovalent interactions," J. Chem. Theory Comput. **10**, 49 (2014).
[120]B. Brauer, M. K. Kesharwani, and J. M. L. Martin, "Some observations on counterpoise corrections for explicitly correlated calculations on noncovalent interactions," J. Chem. Theory Comput. **10**, 3791 (2014).
[121]F. Jensen, "Basis set superposition errors are partly basis set imbalances," J. Chem. Theory Comput. **20**, 767 (2024).

[122]S. Gojare, S. Chen, J. Chen, Z. Yu, J. Vázquez Quesada, P. N. Pleßow, K. Fink, and Y. Wang, "Adsorption of co on α-Al_2O_3(0001): A combined experimental and computational study," ChemPhysChem **26**, e202401134 (2025).
[123]G. Spoto, E. Gribov, A. Damin, G. Ricchiardi, and A. Zecchina, "The IR spectra of Mg^{2+}_{5C} (CO) complexes on the (001) surfaces of polycrystalline and single crystal MgO," Surf. Sci. **540**, L605 (2003).
[124]H.-Z. Ye and T. C. Berkelbach, "Adsorption and vibrational spectroscopy of CO on the surface of MgO from periodic local coupled-cluster theory," Faraday Discuss. **254**, 628 (2024).
[125]J. Maul, G. Spoto, L. Mino, and A. Erba, "Elucidating the strucrure and dynamics of co ad-layers on MgO surfaces," Phys. Chem. Chem. Phys. **21**, 26279 (2019).